Plasticization of Poly(ethylene oxide) in Fluid CO_2 Measured by in-Situ NMR

Louis A. Madsen*

Department of Chemistry, University of North Carolina, Chapel Hill, North Carolina 27599-3290

Received September 29, 2005; Revised Manuscript Received December 13, 2005

ABSTRACT: While use of CO_2 as a solvent for polymer synthesis has been well established, applications to polymer processing have followed more slowly. Motivated by success using supercritical CO_2 as a mediating solvent in forming composites of montmorillonite "nanoclay" with plasticized polymer melts, this study makes a detailed quantification of the CO_2 plasticization of solid poly(ethylene oxide) (PEO) using NMR spectroscopy and relaxation experiments. The study of solid polymers using NMR presents challenges but can yield detailed information about polymer morphology, dynamics, and chemistry. Immersing bulk polymers under fluid CO_2 in an NMR spectrometer allows direct access to plasticization dynamics relevant to polymer processing. Using a simple high-pressure apparatus and temperatures <90 °C, melting and crystallization temperatures are depressed by up to 18 °C when solid PEO is immersed in CO_2 at modest pressures (≤ 82 bar). A detailed analysis of NMR spectral components also quantifies the crystalline/amorphous fractions in PEO as a function of temperature and CO_2 pressure. Thus, this system shows a distinct plasticization effect even at modest CO_2 pressures, emphasizing the utility of CO_2 as a polymer processing aid.

Introduction

Supercritical CO_2 is emerging as an environmentally benign and recoverable solvent in myriad polymer syntheses and processing venues.[1−3] The tunable nature of the supercritical state allows for new degrees of freedom in process design, e.g., pressure, phase transitions, viscosity, and surface tension. Most polymer synthesis and processing protocols involve water or organic solvents, which pose problems of disposal or recycling, and often leave residues in final polymer products that can be toxic or difficult to remove. CO_2 provides an environmentally friendly and economical alternative to many conventional solvent processes. Commercial CO_2 production uses byproducts of other industrial processes and sequesters or adds no additional gas to the atmosphere.[2] CO_2 generally separates easily from products due to its liquid−gas transition when pressure in the reaction or processing vessel is released. CO_2 is known to be a plasticizer for polymers[4,5] and could be used to improve processing for polymers that are difficult to form. Thus, CO_2 may replace some traditional solvent-mediated composite manufacturing, providing better polymer/additive mixing than simple melt mixing, but without the harmful processing solvents. In this study, the properties and utility of CO_2 as a plasticizer are explored by monitoring its effects on an example polymer in real time using solid-state NMR spectroscopy. This work represents the first detailed NMR investigation of a bulk solid polymer under the influence of a CO_2 (fluid) atmosphere.

Recent work has focused on blending polymers with montmorillonite, a so-called "nanoclay" due to its 1 nm silicate layer spacing, using sc-CO_2 as an effective blend-mediating or dispersion-polymerization solvent. This work has utilized hydrocarbon polymers that are only weakly soluble in CO_2, but has found dramatic success in synthesizing both intercalated and exfoliated nanocomposites. In the case of poly(ethylene oxide) (PEO), CO_2 dissolves into the polymer and promotes motion and mixing with the clay to form a uniform composite.[6] Other studies show the effectiveness of dispersion polymerizations of poly(methyl methacrylate) (PMMA) and polystyrene (PS) in CO_2 in the presence of clay to form the composites.[7]

Because of inconveniences in making measurements on a synthesis or processing vessel, most analytical measurements on solid polymers and composites can only infer properties during processing from measurements made only on the final product in the absence of CO_2. To gain direct insight into polymer dynamics, morphology, and chemistry during processing, analysis must be done in situ. Previous studies have used high-pressure differential scanning calorimetry[8] (DSC) and electron spin resonance[5] to assess thermal state changes under the influence of CO_2 and other gases. DSC, IR, variable temperature TEM, and X-ray diffraction can give information on crystallinity,[9] but in-situ plasticization is not generally accessible under high-pressure gases. These methods each provide a different and incomplete set of information on polymer properties, while some require destruction or degradation of the sample.

NMR can provide a wealth of information on the dynamics of polymers, including measuring melting and glass transition temperatures, phase behavior, chemical affinity, and binding, and these properties may be separately measured on the polymer backbone and on chemically distinct side chains.[10] A large body of NMR work exists on polymer and other solutions in CO_2,[11,12] but not previously on *solid* polymers with CO_2 as a dissolved solute. The present NMR study of solid PEO immersed in CO_2 uses a simple and inexpensive high-pressure cell and finds that the melting and crystallization temperatures of this semicrystalline polymer are dramatically reduced by immersion in CO_2 at modest pressures, giving further insight into and impetus for the use of CO_2 as a plasticizer during polymer processing. A detailed analysis of these experiments yields a bulk average amorphous/crystalline fraction during melting[13] and observes strong hysteresis in the melting curve.[14]

Experimental Section

To get reproducible results, the PEO sample (powder, 100 kDa MW, Scientific Polymer Products Inc.) is degassed under vacuum

* E-mail: lmadsen@email.unc.edu.

10.1021/ma052118b CCC: $33.50 © 2006 American Chemical Society
Published on Web 01/21/2006

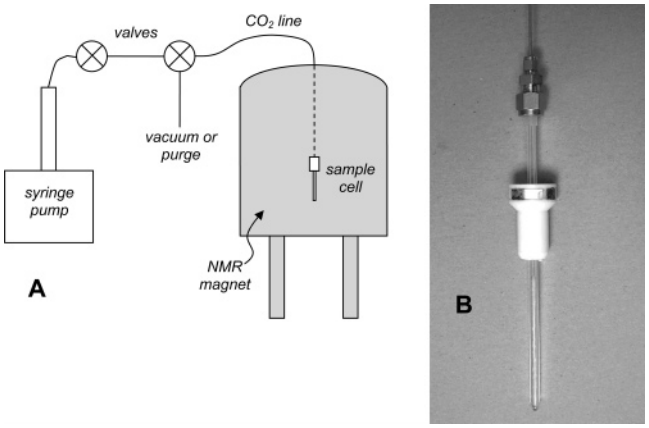

Figure 1. In-situ NMR apparatus. The high-pressure system shown in block diagram (A) connects to the sample cell shown in (B), which resides inside the NMR magnet.

overnight before introduction of CO_2. Most importantly, this removes oxygen from the sample that might influence NMR relaxation times. Also, heat cycling the solid twice before NMR measurements produced more consistent results on repeated measurements on the same sample or between samples. Figure 1 shows the sample cell along with a block diagram of our high-pressure NMR apparatus. The sample cell consists of a 5 mm o.d., 1.4 mm i.d. NMR tube connected to a 0.0625 in. o.d. stainless steel capillary via a swagelok 0.25 in./0.0625 in. adapter and semiflexible nylon tubing (Polypenco Nylaflow 1/4T, 0.63/0.49 cm o.d./i.d.) for a seal. Careful heating using a hot air gun aids installation of the 1.5 cm long nylon tubing section onto the NMR tube. Tightening of the swagelok to NMR tube seal using the swagelok protocol avoids stress cracks in the tube that might cause rupture under pressure. Prior to insertion of the sample cell into the spectrometer, the pump applied a maximum pressure of 88 bar with the cell submersed in a 20 L bucket of water to protect against debris in the event of rupture. A conventional HPLC-type syringe pump (ISCO 100DX pump with Series D controller) applies high pressures, and no ruptures occurred up to 61 bar with glass tubes (Wilmad 522-PP) and up to 88 bar with quartz tubes (Wilmad 700-PQ). Testing on similar glass sample tubes indicates that they burst at an average pressure of 103 bar with a standard deviation of 35 bar.[15] Quartz tubes should have much higher burst pressures, but more testing is needed to determine the maximum safe operating pressure. Because of the possibility of pressure drop along the ~5 m stainless capillary tube, a pressure sensor was attached (Sensotec THE/743-11TJG) to the end of the capillary in place of the sample cell. The drop in pressure relative to the pump was <1 bar after a few minutes of equilibration, so the pressures at the pump are reported as equal to those as in the sample cell. All valves between the pump and sample cell were open during the variable temperature runs to allow for pressure equilibration. Filling the sample cell so that sample lay only inside the NMR coil allowed for more uniform rf excitation and detection.

All data originated from a Bruker Avance DMX 360 MHz solids instrument. ^{1}H NMR experiments used <2 μs pulse widths for uniform spectral excitation and used a standard inversion−recovery pulse sequence (180°−τ−90°−acquire) for all T_1 measurements. Temperature steps equilibrated for >5 min before taking NMR data. Inversion−recovery experiments incorporated relaxation delays of 9 s and 4 scans for each time increment for a total of 12 min per T_1 measurement. A 13-point τ delay sequence provided coverage for T_1's ranging from 0.7 to 2.5 s. For best reproducibility, T scans for cooling−heating cycles began at the highest T seen during each cycle and equilibrated for >15 min before beginning the cycle. A neat ethylene glycol standard sample (Bruker) allowed temperature calibration in 5 °C intervals in the same position in the NMR probe as the high-pressure cell. Repeated measurements provided an estimated T uncertainty of <±0.5 °C using this apparatus.

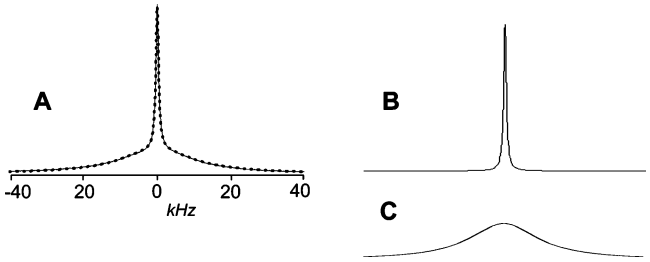

Figure 2. Solid-state NMR spectrum and fit components. Part A shows the spectrum of PEO in CO_2 at 82 bar and 25.7 °C. The data are in the solid line, and the dotted line shows the least-squares fit using two Lorentzian line shapes. Parts B and C are the narrow (amorphous) and broad (crystalline) components derived from the fit. The intensities of (B) and (C) allow calculation of the crystalline and amorphous fractions in the sample.

In conventional CO_2/polymer solution studies where the polymer is distributed throughout the pressure apparatus, the issue of polymer concentration in the sample cell vs in the mixing cell or transfer tubing becomes important. If the NMR spectrometer sets temperature in the sample cell while the rest of the pressure system is at room temperature, then polymer may condense into the cooler part of the system, leaving the sample cell with a different and uncharacterized concentration relative to that originally planned. This is not an issue in our experiments since our sample stays solid in the sample tube and is completely influenced by the NMR probe T. When using a polymer with high solubility in CO_2, some solid may dissolve during the NMR experiment. However, this dissolved polymer would produce only a small contribution to the signal and would not substantially affect the NMR measurements.

To compare classical polymer characterization methods to this NMR method, 8.1 mg of the commercial sample studied using NMR was examined using DSC (Seiko SSC/5200) with heating/cooling rates of 1 °C to 10 °C/min.

Results and Discussion

To illustrate the utility of NMR for polymer studies, a simple line shape analysis allows extraction of the amorphous/crystalline fraction of the PEO as a function of P_{CO_2} and T. Figure 2 shows an example spectrum and its decomposition into two spectral components via least-squares fits of two Lorentzian line shapes to the data using Mathematica 4.1. Note the "broad" and "narrow" components, where the broad component arises from a solid or less mobile crystallite and the narrow component to the more mobile amorphous polymer. What these components represent may differ slightly from other methods of determining crystallinity,[9] since these line shapes really relate to the average *motions* the polymer segments experience. The slowly moving parts correspond to the true crystallites, but there will also be some portion of the polymer moving within or on the surface these crystallites that is not crystalline but has similar motional behavior on the NMR time scale. Thus, the crystalline fraction measured here should be slightly larger than that obtained by other analytical methods.

Because of nonlinearities in the NMR signal intensity over the spectral window arising from the NMR measurements, our fits to the spectral components will have errors larger than the errors calculated by the fitting software. This error will be similar to that expected for using NMR peak areas (integration) to determine relative spin abundances, typically ±5%. This error could be substantially reduced by careful calibration of NMR probe and spectrometer response in both excitation and detection. Figure 3 shows two sets of spectra vs T under cooling at P_{CO_2} = 1 bar and P_{CO_2} = 82 bar (supercritical) with the crystalline fractions shown at left. Notice that the melting of PEO shows metastable behavior, at least on the 0.05 °C/min

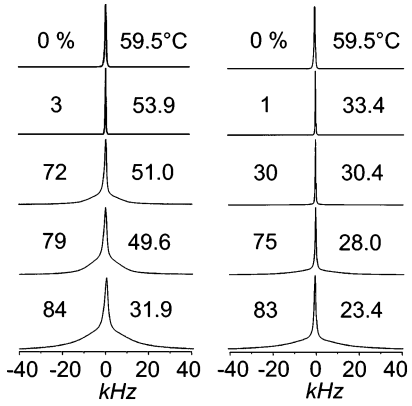

Figure 3. NMR spectra of PEO vs T and P_{CO_2}. The spectra at left were acquired on neat PEO on cooling, while those at right were taken at $P_{CO_2} = 82$ bar. The numbers to the left of each spectrum give the percent crystallinity as determined by the line shape analysis. The intensities of the spectra are individually scaled to allow comparison of the line shapes. Note that the line widths of the narrow (amorphous) spectral components are smaller in the data taken at $P_{CO_2} = 82$ bar, indicating enhanced polymer motion even below the melting temperature of the crystalline part.

average cooling rate used in our experiments. This appears to be stable over quite long time scales, since experiments run at fixed T for >1 h showed no substantial change in crystallinity. Note that the neat polymer is completely amorphous above 54 °C and solidifies over a ~4 °C range.

One may also observe the thermodynamic states of polymers using the spin−lattice relaxation time T_1. NMR relaxation times reflect the exchange of energy of the spins with their local magnetic environments. The spin−lattice relaxation time T_1 is the exponential decay time (1/rate) that the spin system takes to return to thermal equilibrium, manifested as a material sample's bulk average magnetic moment given by the nuclear spin paramagnetism (a Boltzmann population difference) aligned along the spectrometer field axis. Once the spins have been put into a nonequilibrium state, such as with an rf pulse, random spin flips induced by magnetic fluctuations cause the spin system to return to its Boltzmann-distributed equilibrium state. The dominant source of this magnetic "noise" in polymers typically arises from motions of the spins riding on the polymer chains, which have a spectrum of motional frequencies and amplitudes. The spins are coupled to their neighbors by dipole−dipole or other spin interactions. Figure 4a depicts this noise interaction schematically. As the frequency spectrum of the motions (the noise) changes, as a result of, e.g., temperature changes or other physical or chemical changes to the sample, the relaxation time T_1 responds in a quasi-resonant way at the Larmor frequencies of the spins, as depicted in Figure 4b. Thus, we may use T_1 as a probe of phase transitions in a sample, including measuring the phase or motional transitions separately in any chemically distinct groups in a polymer or other substance.

Because T_1 probes polymer motions on the Larmor frequency ω_0 time scale (1/360 MHz in the present work), as the polymer melts or crystallizes T_1 will generally go through a strong transition as the frequency spectrum of motions of the spins in the polymer drastically change. Figure 5a shows a cooling−heating T cycle for PEO with reference to the relevant points in Figure 4b. A similar effect on T_1 should also hold for glass transitions, although the T_1 dependence will be generally weaker with T. Thus, although phase transition measurements occur at ω_0, they will be similar to or only minimally higher than measurements made near zero frequency, such as those obtained using DMA or DSC, especially for strong transitions like melting and crystallization. Corrections for this "frequency offset" when measuring glass transitions may be accomplished using time−temperature superposition to calculate a T_g at zero frequency.[10,16,17]

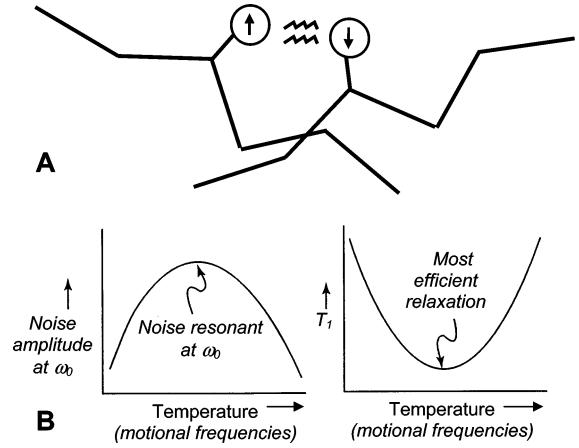

Figure 4. Spin−lattice relaxation times in polymer systems. Part A shows adjacent polymer chains with spins interacting via dipolar interactions, which are modulated by the polymer motional frequencies to produce random dissipative noise that relaxes the spins. Part B shows the quasi-resonant behavior of motions coupling to T_1 as a function of temperature.

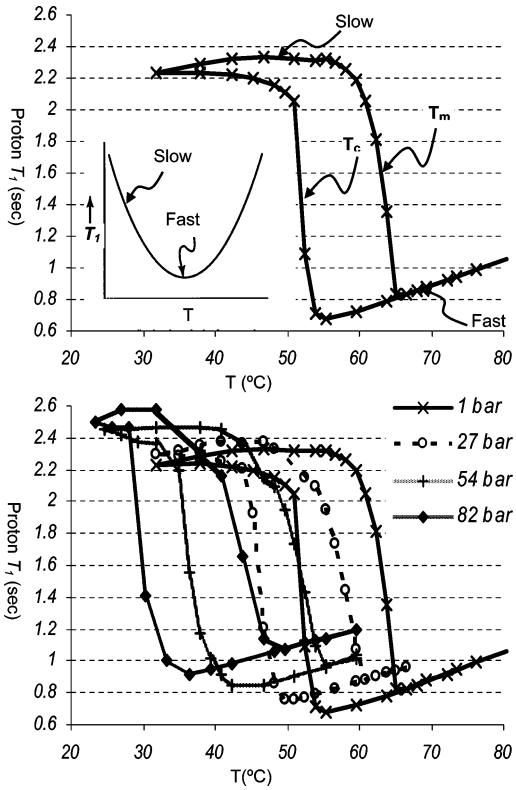

Figure 5. Spin−lattice relaxation times of protons in PEO plasticized by CO_2. The upper plot shows T_1 measurements for a single cooling−heating cycle at $P_{CO_2} \sim 1$ bar. The inset depicts where the slow and fast relaxation measurements fall on the T_1 dependence curve of Figure 4. The T_m and T_c labels denote where the melting and crystallization temperatures lie. The curves in the lower plot show T cycles for a range of P_{CO_2}.

The present study focuses only on melting and crystallization since T_g for PEO is below room T and would presumably decrease with addition of the plasticizer CO_2. Ongoing detailed studies on noncrystalline polymers with higher T_g's and some CO_2 solubility should show similar strong depressions of T_g's.

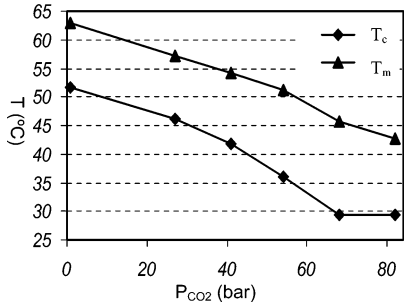

Figure 6. Melting and crystallization temperatures as a function of P_{CO_2}. T_m and T_c of PEO drop monotonically as a function of P_{CO_2}. Note the apparent plateau of T_c when CO_2 becomes a liquid below the critical $T = 31$ °C.

Figure 5b shows a family of curves of the relaxation time T_1 vs T with P_{CO_2} ranging from atmospheric pressure up to 82 bar, which is well above the CO_2 critical pressure. In the present study, the transition temperatures T_m and T_c are defined as melting and crystallization temperatures, respectively, and their values are assigned by taking the midpoint of the T_1 vs T transition based on the values of T_1 in either phase above and below the transition. These curves all show substantial differences between the melting and crystallization temperatures (hysteresis) ranging from 10 °C with no CO_2 to 18 °C at P_{CO_2} = 82 bar, which emphasize the critical role of sample history in thermal processing. Strawhecker and Manias observed this effect using DSC in the absence of CO_2.[14] Note the strong monotonic decrease in both T_m and T_c with increasing P_{CO_2}, which Figure 6 shows graphically. At the low T end of these measurements, below the critical $T = 31$ °C, CO_2 is in the liquid state at $P_{CO_2} \geq 68$ bar, which was confirmed visually as the sample cell exhibited a meniscus with the sample tube as the lowest point in the pressure system during our NMR measurements. This may account for the apparent minimum $T_c = 29.3$ °C observed in these lowest two data points in Figure 6. The 1D spectra of Figure 3 display the growth or disappearance of the broad NMR line, which is an observation of motions on the $^1H-^1H$ dipolar coupling time scale of ~50 kHz. T_m and T_c extracted from these spectral transitions correspond within the estimated temperature accuracy to the T_m and T_c values measured using the T_1 curves of Figure 4. This agreement between the T_1 and line shape measurements is expected since the strong (first order) melting/crystallization phase transitions affect all modes of polymer motion dramatically.

Figure 7 shows the DSC data recorded on the commercial sample used for NMR at several heating/cooling rates.[14] All DSC data represent scans taken on the second or later heating cycles and after >15 min annealing at 80 °C to minimize sample history effects. NMR measurements of T_m and T_c represent measurements of melting/crystallization data at steady state (0.0 °C/min), which cannot be obtained using DSC. Note that the NMR determination of T_m matches the DSC measurement to within error bars at 1 °C/min heating rate. Crystallization evidently requires substantially longer than the DSC time scale (~1 min) since the NMR measurement follows the trend of T_c vs cooling rate but is 3 °C higher than the DSC value at 1 °C/min cooling rate. Indeed, the DSC trace in Figure 7a shows that the crystallization process begins at ~52 °C, exactly where the steady-state NMR measurement of T_c lies.

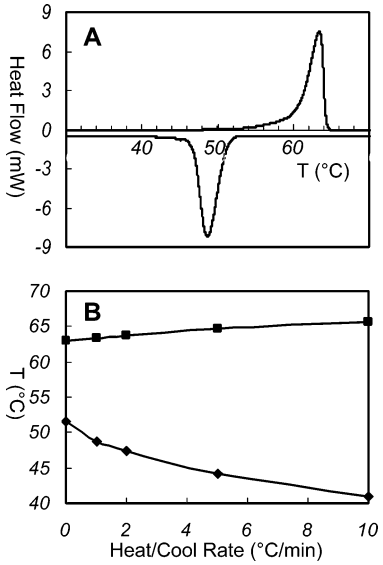

Figure 7. Comparison of DSC with NMR information. Part A shows a differential scanning calorimetry cycle (fourth heat) at 1 °C/min heating/cooling rate. $T_m = 63.3$ °C and $T_c = 48.7$ °C using this method. The data shown in (B) plots T_m and T_c as a function of temperature scan (heat/cool) rate, where the NMR data, essentially at steady state (0.0 °C/min scan rate), provide the data points at 0 scan rate.

Conclusions and Prospects

Assessment of polymer processing methods requires fundamental physical measurements on basic polymer dynamics and interactions with solvents and reactants in realistic conditions. Supercritical CO_2 presents a versatile and environmentally friendly solvent for processing but presents barriers to conventional analysis modes. Using the model polymer system of PEO along with a relatively simple high-pressure NMR apparatus has yielded information relevant to polymer processing techniques such as solvent-mediated polymer composite blending. NMR has no destructive effects on such systems and might be fruitfully integrated into a processing apparatus. The combination of information available from the present study—crystalline/amorphous fraction and melting and crystallization temperatures vs T and P_{CO_2}—also conveniently combines information unavailable from any single analytical technique.

Further plans include applying the present apparatus and methods to study a family of fluoropolymers under development as next-generation photoresists for lithographic processing.[18] Fluoropolymers have much stronger interactions with and higher solubility in CO_2 and have shown more promise as CO_2 synthesis and processing targets. ^{19}F NMR has the added advantage of a much larger chemical shift range in which to distinguish the behaviors of various polymer subunits. In addition, the determination of CO_2 content (wt %) in a solid polymer can likely be quantified using ^{13}C NMR experiments along with a line shape analysis analogous to the present work.

The predominant mode of development for polymer synthesis and processing methods is the use of experience-based intuition, combined with measurement of desired material properties in final products. While this often serves end goals adequately, the use of detailed in-situ analysis techniques allows design to take a more rational and efficient path. This study has depicted a simple method of NMR directed toward understanding in-process parameters of solid polymers plasticized by CO_2. This increasingly important green solvent promises to revolutionize many areas of polymer science as well as chemistry, materials science, and manufacturing.

Acknowledgment. The author thanks Edward T. Samulski for gracious use of laboratory equipment and for editing this manuscript. Alex Chao provided NMR measurement assistance

CDV

early in this project. Funding was provided by NASA Grant NAG-1-2301 and funding and shared equipment from the NSF-STC CERSP under Agreement CHE-9876674.

References and Notes

(1) Wood, C. D.; Cooper, A. I.; DeSimone, J. M. *Curr. Opin. Solid State Mater. Sci.* **2004**, *8*, 325−331.
(2) Young, J. L.; DeSimone, J. M. *Pure Appl. Chem.* **2000**, *72*, 1357−1363.
(3) Jones, C. A.; Zweber, A.; DeYoung, J. P.; McClain, J. B.; Carbonell, R.; DeSimone, J. M. *Crit. Rev. Solid State Mater. Sci.* **2004**, *29*, 97−109.
(4) Mi, Y. L.; Zheng, S. X. *Polymer* **1998**, *39*, 3709−3712.
(5) Harbron, E. J.; Bunyard, W. C.; Forbes, M. D. E. *J. Polym. Sci., Part B: Polym. Phys.* **2005**, *43*, 2097−2108.
(6) Zhao, Q.; Samulski, E. T. *Macromolecules* **2003**, *36*, 6967−6969.
(7) Zhao, Q.; Samulski, E. T. *Macromolecules* **2005**, *38*, 7967−7971.
(8) Zhang, Z. Y.; Handa, Y. P. *J. Polym. Sci., Part B: Polym. Phys.* **1998**, *36*, 977−982.
(9) Gedde, U. W. *Polymer Physics*; Chapman and Hall: New York, 1995.
(10) McBrierty, V. J.; Packer, K. J. *Nuclear Magnetic Resonance in Solid Polymers*; Cambridge University Press: New York, 1993.
(11) Wallen, S. L.; Schoenbachler, L. K.; Dawson, E. D.; Blatchford, M. A. *Anal. Chem.* **2000**, *72*, 4230−4234.
(12) Dardin, A.; Cain, J. B.; DeSimone, J. M.; Johnson, C. S. *Macromolecules* **1997**, *30*, 3593−3599.
(13) Johansson, A.; Tegenfeldt, J. *Macromolecules* **1992**, *25*, 4712−4715.
(14) Strawhecker, K. E.; Manias, E. *Chem. Mater.* **2003**, *15*, 844−849.
(15) Blatchford, M. A.; Wallen, S. L. *Anal. Chem.* **2002**, *74*, 1922−1927.
(16) Williams, M. L.; Landel, R. F.; Ferry, J. D. *J. Am. Chem. Soc.* **1955**, *77*, 3701−3707.
(17) Rubenstein, M.; Colby, R. H. *Polymer Physics*; Oxford University Press: New York, 2003.
(18) Toriumi, M.; Shida, N.; Yamazaki, T.; Watanabe, H.; Ishikawa, S.; Itani, T. *Microelectron. Eng.* **2002**, *61*, 717−722.

MA052118B